INTEGRATING FLOOD HAZARD MAPPING WITH AHP AND MACHINE LEARNING FOR EVALUATING LAND USE PLANNING EFFECTIVENESS: A CASE STUDY IN HA TINH, VIETNAM

Tran Trong Phuong[1], Le Thi Lan[2]

[1]*Faculty of Natural Resources and Environment, Vietnam National University of Agriculture, Ha Noi, Vietnam*

[2] *Faculty of Land Management, Hanoi University of Natural Resources and Environment, Ha Noi, Viet Nam*

Email: ttphuong@vnua.edu.vn

ABSTRACT:

Flooding is among the most destructive natural hazards in Vietnam, frequently causing widespread damage to livelihoods, infrastructure, and ecosystems. This study proposes an integrated framework that combines the Analytic Hierarchy Process (AHP) with machine learning to improve flood hazard mapping and evaluate the effectiveness of land use planning in Ha Tinh province. Six indicators in cluding proximity to stream, slope, elevation, aspect, land use/land cover, and precipitation were selected and weighted using AHP. To enhance objectivity, the Support Vector Machine (SVM) model was trained using stratified random samples yielding probability-based susceptibility maps with improved predictive accuracy. The flood risk map indicated that nearly two-thirds of the province is classified as high or very high flood risk, with the “very high risk” zone alone covering 3,011.27 km² (47.66%) and the “high risk” zone 1,089.38 km² (17.24%). Overlay analysis with the 2030 land use planning map revealed that 4,100.65 km² of planned land lies within high flood risk zones, including 2412.12 km² of forest land, 622.83 km² of paddy land, and 613.77 km² of residential land. These results highlight critical conflicts between future land use development and flood hazard exposure. The findings underline the urgent need to incorporate disaster risk reduction and climate change adaptation into land use planning, while also demonstrating the potential of the AHP and machine learning framework as a transferable tool for flood-prone regions.

Keywords: *Flood risk mapping, Analytic Hierarchy Process (AHP); Machine learning; Support Vector Machine (SVM); Ha Tinh Province; Spatial planning; Sustainable land management.*

1. INTRODUCTION

Flooding is widely recognized as one of the most destructive natural hazards globally, posing significant threats to human life, property, agriculture, and ecosystems (Jonkman, 2005; Kundzewicz et al., 2013; Glago, 2021). According to international disaster reports, floods account for a large proportion of natural disaster related damages each year, not only in terms of economic losses but also in terms of social disruption and environmental degradation (Svetlana et al., 2015; Istomina &

Dobrovoski, 2016). In developing countries, the consequences are often more severe due to limited infrastructure, insufficient early-warning systems, and rapid population growth in flood-prone areas (Perera et al., 2020, Kiptum et al., 2025; Ringo et al., 2025).

Vietnam, located in a tropical monsoon climate zone, is highly vulnerable to hydro-meteorological hazards, particularly floods (Hoang et al., 2019; Nguyen et al., 2021). The North Central Coast, where Ha Tinh province is situated, experiences heavy seasonal rainfall, frequent typhoons, and complex river systems that make the region prone to recurrent flooding (Pham et al., 2018; Ortiz-Vargas & Sebesvari, 2021). Historical records indicate that Ha Tinh has suffered multiple large-scale flood events over recent decades, causing substantial damage to infrastructure, agriculture, and local livelihoods. The province's geographical characteristics, including mountainous areas in the west and low-lying plains along the coast, further increase its exposure to flood hazards (Le et al., 2023; Nguyen et al., 2023).

Rapid socio-economic development has also contributed to the intensification of flood risks (Gu et al., 2020; Yin et al., 2021; Ullah et al., 2025). The expansion of industrial zones, infrastructure projects, and urban areas has led to significant land-use changes, reducing natural water retention capacity and increasing surface runoff (Xu et al., 2020; Bojer et al., 2025). At the same time, climate change is projected to intensify rainfall extremes and sea-level rise, which are likely to exacerbate flood frequency and severity in the coming decades (Kirshen et al., 2008; Goodess, 2013; Rajkhowa & Sarma, 2021). These combined natural and anthropogenic pressures underline the urgent need for comprehensive flood risk assessment in the province (Le et al., 2021; Loi et al., 2022).

In recent years, advances in remote sensing and Geographic Information Systems (GIS) have provided new opportunities for flood risk mapping (Dano Umar et al., 2011; Wang & Xie, 2018; Amatebelle et al., 2025). The Analytic Hierarchy Process (AHP) has been widely applied as a multi-criteria decision-making approach to assign weights to various flood-related indicators, producing expert-driven risk maps (Ghosh & Kar, 2018; Goumghar et al., 2025; Singha et al., 2025). However, while AHP is transparent and systematic, it is also subjective and may not fully capture complex, nonlinear interactions between indicators (Munier & Hontoria, 2021). In contrast, machine learning algorithms have demonstrated strong capabilities in classification and prediction, allowing for data-driven modeling of flood susceptibility (Zhou et al., 2023; Al-Kindi et al., 2024).

This study proposes an integrated framework that combines AHP with machine learning to produce reliable flood risk maps for Ha Tinh province. The AHP method is first applied to establish a structured hierarchy of indicators and compute their relative importance, generating an initial risk map. Training samples derived from this map are then used to build machine learning models, which output probability-based susceptibility maps. Finally, the results of both approaches are compared and validated to ensure robustness. By adopting this dual methodology, the research aims to enhance

the accuracy of flood risk assessment and provide scientific evidence to support disaster risk management and sustainable land-use planning in Ha Tinh and similar flood-prone regions of Vietnam.

2. MATERIALS AND METHODOLOGY

2.1. Study area

The study was conducted in Ha Tinh Province, located in the North Central region of Vietnam (Figure 1). The province covers a natural area of about 6,055 km², bordered by Nghe An Province to the north, Quang Binh Province to the south, the Lao People's Democratic Republic to the west, and the East Sea to the east. Ha Tinh has a population of approximately 1.3 million (GSO, 2024), with livelihoods primarily dependent on agriculture, forestry, aquaculture, and small-scale industries. Following administrative restructuring in 2025, the province comprises 69 communes and wards under a simplified two-tier governance model.

Topographically, Ha Tinh displays a distinct west–east gradient, ranging from mountainous headwater areas in the west (e.g., Son Kim, Vu Quang, Huong Khe) to low-lying plains and coastal zones in the east (Thach Khe, Cam Binh, Ky Anh). The province has a dense river network, with major systems such as the La, Ngan Sau, and Ngan Pho Rivers draining toward the East Sea. This diverse terrain, combined with a tropical monsoon climate and high annual rainfall exceeding 2,000 mm, contributes to frequent flooding and other water-related disasters (Le et al., 2021). Moreover, rapid socio-economic development—including the expansion of industrial zones, transportation networks, and the Vung Ang deep-sea port—has intensified land-use pressures and altered flood susceptibility patterns across the province (Loi et al., 2022).

Overall, Ha Tinh serves as a representative case study for flood risk assessment in Vietnam's central region, where natural conditions and human activities interact dynamically to shape flood exposure and vulnerability.

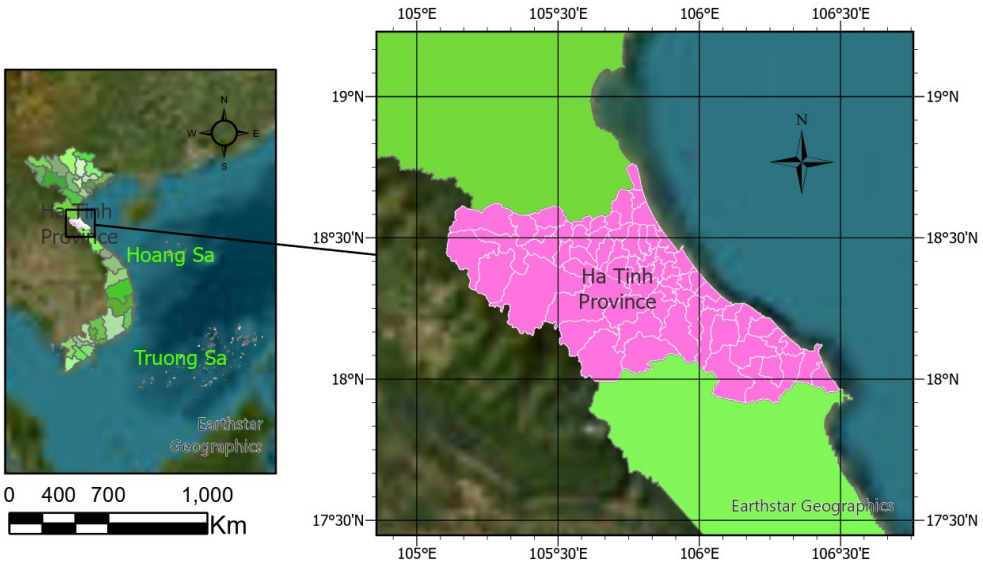

Figure 1: Location of the study area

2.2. Data sources

This study employed a combination of remote sensing products and ancillary datasets to derive the indicators used for flood risk assessment. Six primary data sources were collected, each corresponding to one of the selected indicators:

- Hydrological data: The river network is taken from the Ministry of Agriculture and Environment data source, providing vector river layers used to generate distance rasters from near to the river.

- Topographic data: The topographic data were obtained from the ALOS World 3D DEM (AW3D30, 12.5 m) provided by Japan Aerospace Exploration Agency (JAXA), accessed through the Google Earth Engine using the command:

(ee.Image("JAXA/ALOS/AW3D30/V3_2")).

- Land use/land cover (LULC): Land cover information was obtained from a Sentinel-2 satellite image land cover classification map collected on April 2, 2025, providing detailed land cover classes across the study area.

- Precipitation: Annual rainfall data were compiled from the Climate Hazards Group InfraRed Precipitation with Station data, aggregated from daily observations at ~5 km resolution (Funk et al., 2015).

- Administrative boundary: Vector boundary of Ha Tinh province is taken from the database of the Ministry of Agriculture and Environment for convenient cutting and displaying results.

- Infrastructure data: Land use planning maps were collected from the Department of Agriculture and Environment for contextual analysis.

All datasets were projected to a common coordinate system (EPSG:4326) and resampled to consistent spatial resolution prior to analysis. The integration of multi-source datasets from global repositories and national agencies ensured both spatial detail and thematic accuracy for constructing flood risk indicators.

2.3. Methodology

The research process is designed to combine the Analytic Hierarchy Process (AHP) method with machine learning algorithms to build a flood risk map systematically and objectively. The entire data processing steps are shown in Figure 2, including the following main stages:

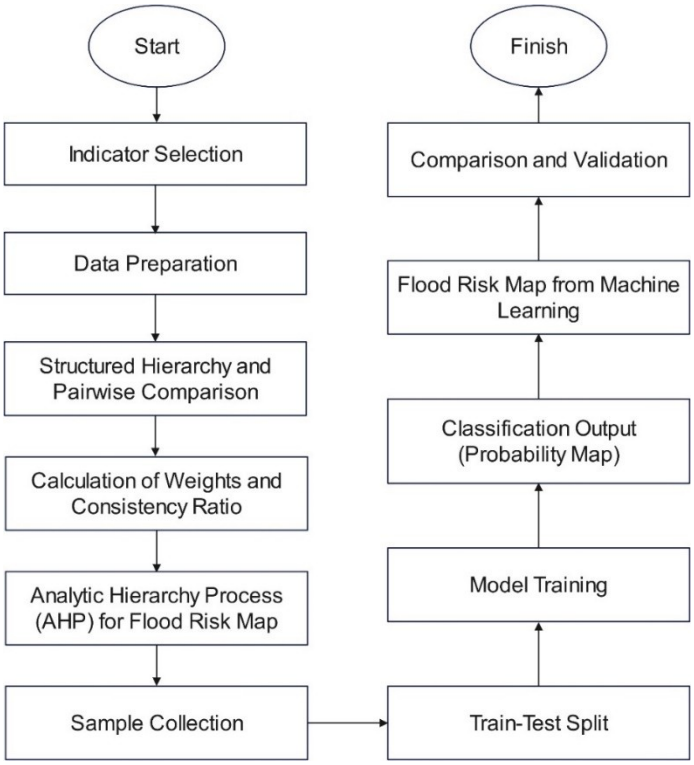

Figure 2: Flowchart of data processing in this study

2.3.1. Indicator selection

In the development of a flood risk map, the initial and fundamental step is the selection of indicators that can effectively represent the key factors influencing flood hazards. This selection is based on theoretical foundations regarding the impacts of natural, anthropogenic, and hydro-meteorological conditions on flood occurrence, supported by previous research findings and the availability of reliable datasets (Kılıç & Bektaş Balçık, 2025). Six major indicators were identified for this study:

(i) Proximity to stream, which reflects the higher flood susceptibility of areas located close to river networks;

(ii) Slope, a crucial factor determining surface runoff velocity and water accumulation capacity;

(iii) Elevation, which indicates the vulnerability of low-lying areas to inundation compared to flood water levels;

(iv) Aspect, related to wind direction and rainfall distribution, thereby indirectly affecting surface flow concentration;

(v) Land use/land cover (LULC), which distinguishes differences in infiltration and water retention capacity across land cover types, influencing flood dynamics;

(vi) Precipitation, a direct meteorological driver of flooding intensity and frequency.

The integration of these indicators ensures a comprehensive assessment, simultaneously capturing the natural baseline conditions and human environment interactions, thereby providing a robust scientific foundation for subsequent analytical steps in flood risk evaluation.

2.3.2. Data preparation

In this step, all selected indicators were collected, standardized, and prepared for analysis. Proximity to stream was generated by rasterizing the river network and calculating the Euclidean distance to the nearest river. Elevation, slope and aspect were derived from the ALOS World 3D DEM provided by JAXA. Land use/land cover (LULC) was constructed using Sentinel-2 imagery acquired on April 2, 2025, classified by three machine learning algorithms (Support Vector Machine (SVM), Random Forest (RF), and Classification and Regression Tree (CART)). Among these models, RF achieved the highest and most reliable classification accuracy, and its results were therefore selected as the LULC input layer for flood susceptibility mapping. The mean annual rainfall was calculated from the CHIRPS daily precipitation data averaged over the period from January 2020 to September 2025, representing the multi-year and near-real-time rainfall conditions of the study area. All datasets were clipped to the study area, projected to EPSG:4326, and resampled to a uniform spatial resolution of 10 m for subsequent analyses.

To make indicators comparable, values are normalized using the min max method (Mazziotta & Pareto, 2022):

$$X' = \frac{X - X_{min}}{X_{max} - X_{min}} \tag{1}$$

where X' is the normalized value, ranging from 0 to 1. This procedure removes unit differences (for example, slope in degrees, elevation in meters, precipitation in millimeters) and ensures equal contribution of each factor. The processed and normalized layers are then exported and validated, forming a consistent dataset for subsequent AHP analysis.

2.3.3. Structured hierarchy and pairwise comparison

In this step, the selected indicators are organized into a hierarchical structure that reflects the overall objective, the evaluation criteria, and their respective sub-factors. At the top level, the objective is to assess flood risk, while the second level consists of the six chosen indicators: proximity to stream, slope, elevation, aspect, land use/land cover, and precipitation. The Analytic Hierarchy Process (AHP) is then applied to quantify the relative importance of each indicator through pairwise comparisons.

In the pairwise comparison method, experts or prior studies are used to assign preference values on a scale from 1 to 9, where 1 denotes equal importance and 9 denotes extreme preference of one factor over another. These judgments form a pairwise comparison matrix $A = [a_{ij}]$, in which each element a_{ij} represents the importance of indicator i compared to indicator j, and the reciprocal property $a_{ij} = 1/a_{ji}$ holds (Kwiesielewicz & Van Uden, 2004).

From this matrix, the normalized principal eigenvector provides the weights of the indicators (Sabzi & King, 2015):

$$w_i = \frac{\lambda_i}{\sum_{j=1}^{n} \lambda_j} \quad (2)$$

where w_i is the weight of indicator i and λ_i is the eigenvalue associated with the comparison matrix. To verify the consistency of expert judgments, the Consistency Index (CI) and Consistency Ratio (CR) are calculated (Aguarón & Moreno-Jiménez, 2003):

$$CI = \frac{\lambda_{max}}{n-1} \quad (3) \qquad CR = \frac{CI}{RI} \quad (4)$$

where λ_{max} is the maximum eigenvalue of the matrix, n is the number of indicators, and RI is the Random Index based on matrix size. A CR value less than 0.1 indicates acceptable consistency (Sato & Tan, 2023). Through this process, the relative weights of the indicators are determined in a systematic and logical manner, ensuring that the subsequent flood risk index reflects both expert knowledge and a mathematically consistent framework. To enhance reliability, the pairwise comparison matrices were developed through consultation with nine experts representing three domains: hydrology and water resources (3 experts), GIS and remote sensing (3 experts), and land-use management and spatial planning (3 experts). Each expert independently evaluated the six indicators using the Saaty 1–9 scale, and individual consistency ratios (CR) were computed. Matrices with CR > 0.1 were discussed and adjusted to achieve acceptable consistency. The geometric mean of the consistent matrices was then used to obtain the final indicator weights, ensuring balanced integration of hydrological, spatial, and planning perspectives.

The selected number of experts follows widely accepted methodological recommendations for AHP applications: 3–5 experts for small-scale studies (Saaty, 2008), 7–12 for provincial or regional studies such as Ha Tinh (Forman & Gass, 2001; Luu et al., 2020), and 15–20 for national-scale analyses (Vargas, 2010; Rahmati et al., 2021). This expert panel structure guarantees both methodological rigor and contextual relevance for the provincial-scale flood assessment.

2.3.4. Calculation of weights

Based on the results of the pairwise comparison matrix and the eigenvector method, the relative weights of the six indicators were derived. These weights represent the degree of influence each factor has on flood risk within the study area. The calculation ensures that all weights sum to 1, thereby enabling a weighted linear

combination of the normalized indicators. In this study, the final weights obtained were as follows: proximity to stream (0.523), slope (0.193), land use/land cover (0.152), elevation (0.054), aspect (0.037), and precipitation (0.040) (Table 1).

These values indicate that proximity to stream is the most influential factor, reflecting the high vulnerability of areas located near major waterways. Slope and land use/land cover follow as important determinants, capturing the role of surface runoff dynamics and human modifications of the landscape. By contrast, elevation, aspect, and precipitation contribute less but remain essential in providing a comprehensive assessment of flood susceptibility ((Kılıç & Bektaş Balçık, 2025). These weights serve as critical inputs for constructing the Flood Risk Index in the following step, ensuring that each indicator contributes proportionally to its relative importance.

Table 1. The weights of the indicators

Indicators	**Proximity to stream**	**Slope**	**LULC**	**Elevation**	**Aspect**	**Precipitation**	**Weight**
Proximity to stream	1	5	6	7	7	9	0.524
Slope	1/5	1	2	5	5	5	0.193
LULC	1/6	1/2	1	5	5	5	0.152
Elevation	1/7	1/5	1/5	1	3	1	0.054
Aspect	1/7	1/5	1/5	1/3	1	1	0.037
Precipitation	1/9	1/5	1/5	1	1	1	0.040
Sum of weights	1.000						
CR	0.078						

2.3.5. AHP Flood Risk Index

Using the AHP-derived weights, the normalized indicator layers are combined into a single Flood Risk Index (FRI) via a weighted linear combination (WLC). Let $P, S, L, E, A, R \in [0,1]$ denote the min max normalized rasters of proximity to stream, slope, land use/land cover, elevation, aspect, and precipitation, respectively; and let the corresponding weights be $w_P = 0.524, w_S = 0.193, w_L = 0.152, w_E = 0.054, w_A = 0.037, w_R = 0.040$ (with $\sum w_i = 1$). The index is computed for each pixel as:

$$\mathrm{FRI} = w_P P + w_S S + w_L L + w_E E + w_A A + w_R R \quad (5)$$

To aid interpretation and stabilize across scenes, the aggregated FRI can be re-normalized to [0,1] (Ghosh & Kar, 2018):

$$\mathrm{FRI}' = \mathrm{FRI} - min\frac{(¿\,\mathrm{FRI})}{max(¿\,\mathrm{FRI}) - min(¿\,\mathrm{FRI})¿¿}¿ \quad (6)$$

The continuous index is discretized into five susceptibility classes for mapping and reporting. A equal-interval scheme (Thammaboribal et al., 2025):

- Low Risk: $0.0 \le \mathrm{FRI}' < 0.2$
- Moderate Risk: $0.2 \le \mathrm{FRI}' < 0.4$
- Risky: $0.4 \le \mathrm{FRI}' < 0.6$

- High Risk: $0.6 \leq FRI' < 0.8$
- Very High Risk: $0.8 \leq FRI' \leq 1.0$

This step yields the AHP-based flood risk map, which serves both as a standalone product and as a basis for sampling/labeling in the subsequent machine-learning workflow.

2.3.6. Sample collection

Once the AHP-based flood risk map is generated, the next step is to collect representative samples that will serve as training and validation data for machine learning models. In this study, the classified flood risk map derived from AHP was used as a reference layer to extract samples from areas with contrasting risk levels. Specifically, regions identified as very low risk (class 1) and very high risk (class 5) were selected to create two distinct classes. This approach ensures that the machine learning model can learn clear patterns distinguishing safe zones from hazardous zones (Wang et al., 2025).

Sampling was carried out using a stratified random approach, in which a predefined number of points were distributed proportionally across the selected risk classes. Specifically, 1000 points were drawn from the low risk class and another 1000 points from the very high risk class. Each sampled point inherited the spectral and thematic information from the six normalized indicators (proximity to stream, slope, land use, elevation, aspect, and precipitation) and was assigned a binary label: “0” for low risk areas and “1” for very high risk areas.

To avoid bias and overfitting, the combined dataset of 2000 samples was then randomly split into two subsets: 70% for training and 30% for testing. This division balances the need for sufficient training data with the requirement for independent evaluation (Zha et al., 2025). By leveraging the AHP-based map as a sampling guide, this step establishes a consistent and scientifically grounded training dataset, ensuring that the subsequent machine learning models are both well-informed and objectively validated.

2.3.7. Feature stack

After collecting and labeling the training and validation samples, the next step is to construct the feature stack, which integrates all selected indicators into a single multi-band dataset. Each band in this stack corresponds to one normalized indicator: proximity to stream, slope, land use/land cover, elevation, aspect, and precipitation. By combining these layers, each sample point or pixel is represented by a vector of six values, reflecting the multi-dimensional conditions that influence flood risk. In practice, this was achieved by concatenating the normalized raster layers into one composite image using Google Earth Engine. The resulting dataset ensures that every spatial location within the study area has consistent and co-registered values across all indicators. Normalization guarantees that the features are dimensionless and lie within the range [0,1], preventing disparities in scale from biasing the model (Singh & Singh,

2022). The feature stack is then used to extract values for the sample points obtained in Step 6. Each point thus forms a record in the training dataset, with six predictor variables (the indicators) and one response variable (the flood risk class). This structured dataset is essential for supervised machine learning, as it allows algorithms to learn patterns that link the multi-indicator conditions to observed flood susceptibility (Ireland et al., 2015).

2.3.8. Model training

After preparing the feature set and the labeled training samples, this study applied three supervised machine learning algorithms integrated within the Google Earth Engine (GEE) platform to predict the probability of flood occurrence. These algorithms include Random Forest (RF), Support Vector Machine (SVM), and Artificial Neural Network (ANN).
The evaluation results indicated that all three models achieved high to very high classification accuracy, among which the SVM model produced the best performance with an overall accuracy (OA) of 91% and a Kappa coefficient of 0.89, demonstrating its superior capability in distinguishing different flood risk levels. These findings are consistent with previous research, which has confirmed that SVM often outperforms other classifiers in flood susceptibility mapping due to its robustness and generalization ability (Nguyen et al., 2024; He et al., 2025; Arora et al., 2025).

In this study, the Radial Basis Function (RBF) kernel was employed to effectively capture nonlinear relationships between predictor variables and flood hazard classes—an approach proven effective for handling complex spatial decision boundaries in environmental modeling (Tehrany et al., 2015; Pham et al., 2020; Hashim et al., 2021; Chen et al., 2022; Mosavi et al., 2023; Das & Chatterjee, 2024). The kernel function is expressed as (Tehrany et al., 2015; Pham et al., 2020):

$$K(x_i, x_j) = \exp\left(-\gamma \| x_i - x_j \|^2\right) \quad (7)$$

Where x_i and x_j are feature vectors, and γ is the kernel parameter controlling the influence of a single training sample. The cost parameter C balances the trade-off between maximizing the margin and minimizing classification error. In this study, γ = 0.1 and C = 100 were selected after preliminary testing. The model outputs class probabilities, which provide a continuous measure of flood risk. The training dataset (70% of samples) was used to fit the models, while the remaining 30% served as an independent test set. Both classifiers were set to output probability surfaces, which were later converted into susceptibility classes. This step enables the machine learning models to generalize from the labeled samples and generate spatially continuous flood risk maps across the study area (Antzoulatos et al., 2022).

2.3.9. Classification output

After training the machine learning models, the next step is to generate spatially continuous flood susceptibility maps by applying the trained classifiers to the entire

feature stack. In the SVM model, the RBF kernel outputs a probability value between 0 and 1, representing the likelihood of flood risk at each location.

To make the results more interpretable, these continuous probability surfaces are transformed into discrete susceptibility classes. A five-level classification scheme was adopted, with thresholds defined as follows (Thammaboribal et al., 2025):

- Low Risk: $0.0 \leq P < 0.2$
- Moderate Risk: $0.2 \leq P < 0.4$
- Risky: $0.4 \leq P < 0.6$
- High Risk: $0.6 \leq P < 0.8$
- Very High Risk: $0.8 \leq P \leq 1.0$

where P is the model-derived probability of flood risk. This classification approach ensures consistency with the AHP-based flood risk map. The classified output is visualized using a color palette ranging from green (low risk) to red (very high risk), which highlights spatial patterns of vulnerability across the study area. The raster maps are also exported in a standard coordinate system (EPSG:4326) for further analysis, reporting, and integration into Geographic Information Systems (GIS). By converting probabilistic outputs into susceptibility categories, this step bridges the gap between statistical modeling and practical decision-making, providing stakeholders with actionable spatial information on flood hazards.

2.3.10. Comparison and validation

The final step of the methodology involved comparing and validating the results obtained from the AHP-based approach combined with the machine learning model. This step ensured that the generated flood risk maps were both reliable and scientifically sound. Validation was performed using an independent test dataset (30 % of the total samples) excluded from the training process. For each validation point, the predicted class values were extracted from the machine-learning-based flood risk map and compared with their actual labels to compute standard accuracy metrics. The key performance indicators included overall accuracy (OA) and the Kappa coefficient derived from the confusion matrix (Congalton, 1991; Foody, 2002).

In addition to statistical validation, spatial comparisons were conducted by overlaying the flood risk maps with the province's current land-use and planning maps to identify and analyze key vulnerable areas. Recent studies have emphasized the importance of rigorous quantitative validation—using OA and Kappa—together with spatial assessment to ensure the practical applicability of flood susceptibility mapping based on hybrid GIS–machine learning frameworks (Antzoulatos et al., 2022; Seydi et al., 2023; Mhangara et al., 2025; Arora et al., 2025).

3. RESULTS AND DISCUSSION

3.1. Land use and topographic characteristics of Ha Tinh Province

The land use and topographic structure of Ha Tinh Province illustrate the interaction between natural geomorphology and land-use transformation (Figure 3). Agricultural land remains dominant, accounting for about 41% of the provincial area, followed by forest and shrubland (36%), while built-up and industrial zones cover around 13% (MONRE, 2024). This composition reveals a transition from upland forest ecosystems to intensively cultivated and urbanized coastal plains. The province's terrain forms a distinct west–east gradient, with three main zones: The mountainous zone (e.g., Son Kim 1, Son Kim 2, Vu Quang, Huong Binh, Huong Khe, Huong Xuan, Mai Hoa) lies above 800 m a.s.l., dominated by steep slopes and dense forests that maintain slope stability and regulate watershed hydrology (Nguyen & Pham, 2022; Tran et al., 2021); The midland transition zone (e.g., Toan Luu, Viet Xuyen, Tung Loc, Gia Hanh, Truong Luu) includes undulating hills and mixed agricultural–forest land, serving as a buffer between uplands and floodplains;The coastal plain zone (e.g., Thach Khe, Thach Lac, Dong Tien, Cam Binh, Cam Xuyen, Ky Anh, Ky Xuan) is a low-lying region shaped by alluvial deposition and intensive human modification.

Hydrologically, this geomorphic sequence determines the pattern of runoff concentration and flood retention across the province. The combination of flat topography, dense infrastructure, and land conversion in the coastal communes amplifies flood susceptibility (Vo et al., 2022; Antzoulatos et al., 2022). Conversely, the upland and midland areas retain higher infiltration capacity due to extensive vegetation and forest cover, mitigating downstream flood peaks.

The land use/land cover (LULC) structure comprises eight surface categories—tree cover, shrubland, grassland, cropland, built-up area, bare vegetation, water bodies, herbaceous wetland, and mangroves (Figure 3). Tree cover and shrubland, concentrated in the western uplands and midland zones, contribute to slope stability and effective water regulation. In contrast, cropland and built-up areas, which dominate the coastal plains, limit infiltration and enhance surface runoff accumulation. Wetlands and mangroves distributed along estuarine and tidal zones act as natural buffers that moderate flood peaks and tidal surges. The spatial distribution of these classes illustrates the strong correlation between topographic gradients, land cover characteristics, and flood susceptibility patterns across Ha Tinh Province.

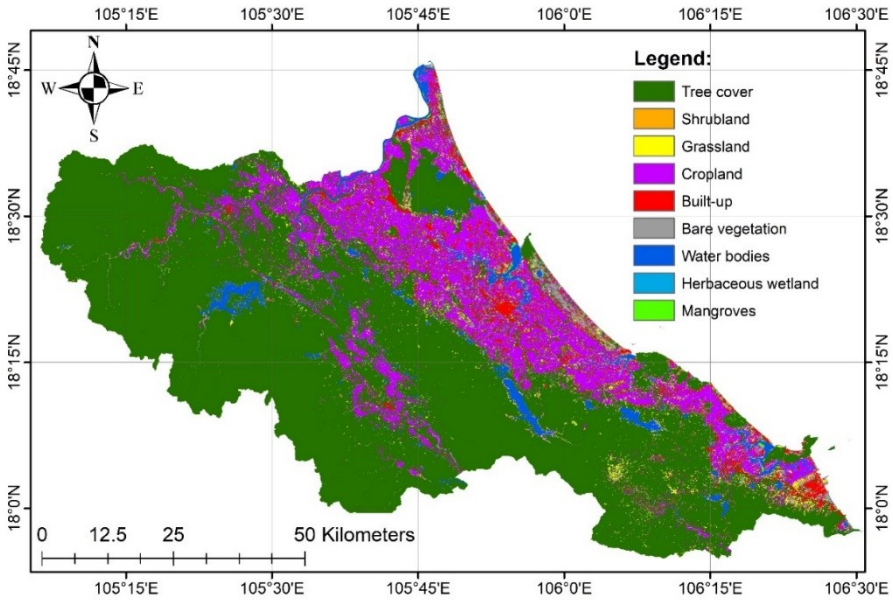

Figure 3: Land use/cover map of Ha Tinh Province

3.2. Spatial indicators and flood susceptibility analysis

Along with the LULC dataset, five spatial indicators—distance to rivers, slope, elevation, aspect, and precipitation (Figures 4–8)—were standardized to a common scale to evaluate their influence on flood susceptibility across Ha Tinh Province. The spatial analysis revealed distinct differences in flood exposure among the province's geomorphological zones.

Coastal and low-lying plains, including communes such as Thach Lac, Dong Tien, Thach Khe, Cam Binh, Ky Anh, and Ky Xuan, exhibit the highest flood exposure levels. These areas are characterized by flat terrain (slope < 5°), low elevation (< 25 m a.s.l.), and proximity to major rivers, estuaries, or the coastline (< 1 km). Such conditions restrict natural drainage capacity while increasing the risk of storm surge and widespread inundation during the monsoon season.

The midland and transitional zones show moderately lower flood susceptibility due to higher elevation and steeper slopes. However, localized flooding can still occur in downstream catchments where runoff converges from upland areas, particularly during peak rainfall months.

The western mountainous communes, including Huong Khe, Huong Pho, and Huong Xuan, display low flood susceptibility. Steep slopes facilitate rapid water discharge, while high forest cover enhances infiltration and reduces surface runoff. Nevertheless, these areas remain vulnerable to flash floods and landslides under prolonged heavy rainfall conditions.

Additionally, annual precipitation exceeding 2,000 mm in the western highlands intensifies surface runoff from upland to lowland regions, exerting hydrological pressure on downstream floodplains. This explains why flood events are typically more severe and prolonged in coastal and deltaic areas compared with the uplands.

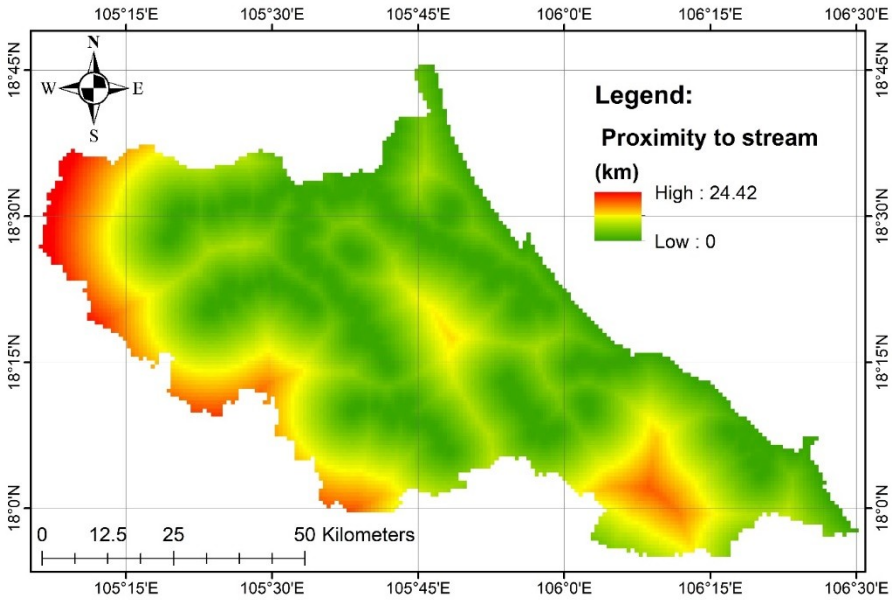

Figure 4: Proximity to stream map of the study area

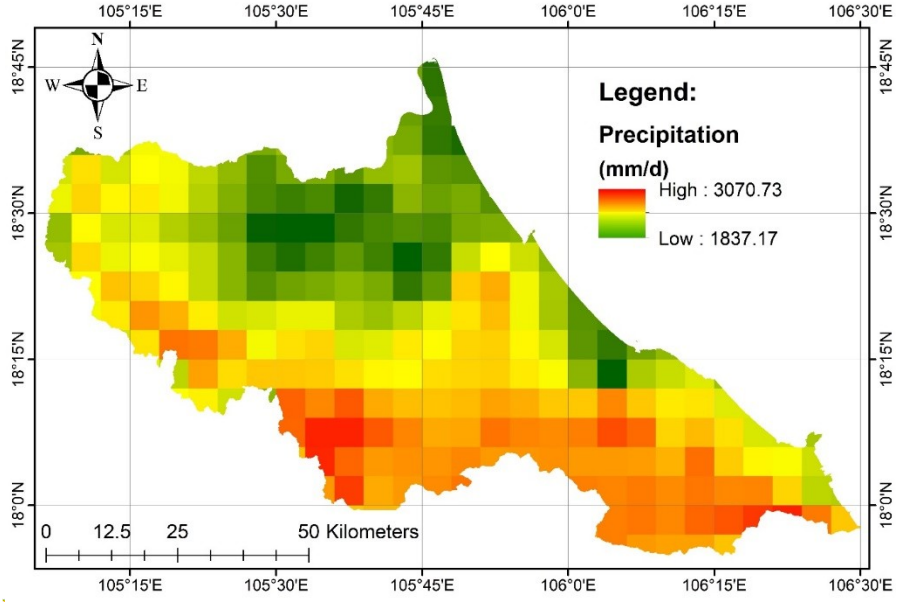

Figure 5: Precipitation map of the study area

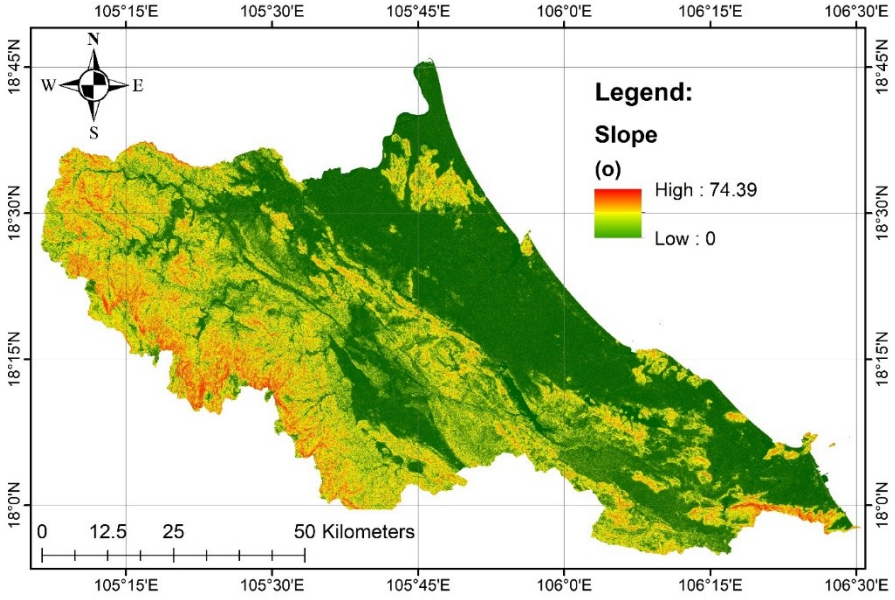

Figure 6: Slope map of the study area

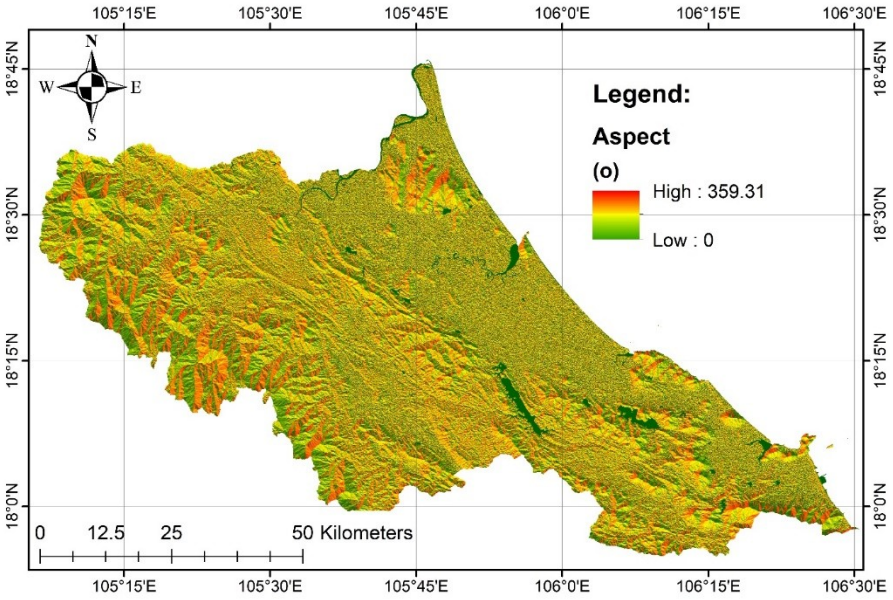

Figure 7: Aspect map of the study area

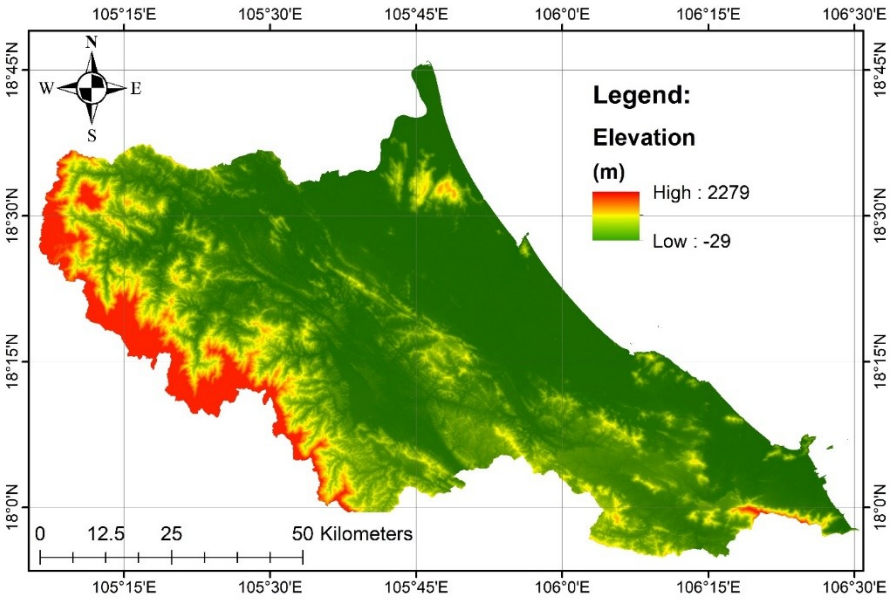

Figure 8: Elevation map of the study area

3.3. Weighting of flood-related indicators (AHP results)

The relative importance of the six indicators—proximity to river, slope, elevation, aspect, land use/land cover, and precipitation—was determined using the Analytic Hierarchy Process (AHP) based on expert consultation (Figure 9). Nine experts representing hydrology (3), GIS and remote sensing (3), and land-use planning (3) conducted pairwise comparisons using the Saaty 1–9 scale. Individual consistency ratios (CR) were computed, and matrices with CR > 0.1 were refined through group discussion to achieve acceptable coherence. Final weights were derived from the geometric mean of all consistent matrices.

According to the results, proximity to river (0.524) had the highest weight, highlighting its dominant influence on flood susceptibility. Slope (0.193) and land use/land cover (0.152) followed as key contributors, confirming the strong geomorphic and anthropogenic control over flood dynamics. The calculated Consistency Ratio (CR = 0.078) satisfied the acceptable limit (<0.1), ensuring logical reliability of expert judgments. The adopted expert panel size (9 specialists) conforms with international AHP recommendations: 3–5 experts for small-scale studies (Saaty, 2008), 7–12 for provincial or regional analyses (Forman & Gass, 2001; Luu et al., 2020), and 15–20 for national-level assessments (Vargas, 2010; Rahmati et al., 2021).

These validated weights were subsequently applied to compute the flood hazard index, providing a balanced integration of hydrological, spatial, and land-use factors for subsequent modeling.

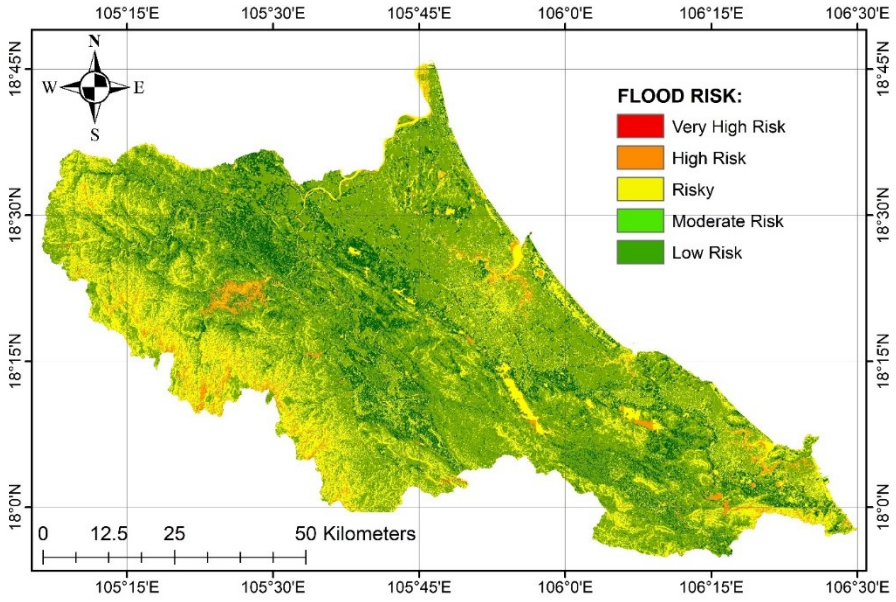

Figure 9: Weights of flood-related indicators derived from AHP

3.4. Flood risk mapping from AHP and machine learning

The AHP-derived and SVM-based flood risk maps (Figure 10) exhibit strong spatial consistency, with the integrated model providing a refined delineation of flood-prone zones across Ha Tinh Province. The hybrid AHP–SVM model significantly improved classification performance compared to AHP alone (OA = 0.87; Kappa = 0.81), confirming the effectiveness of combining expert-based and data-driven approaches. This integration allowed the model to capture nonlinear interactions among topography, rainfall, and land cover, which are typically oversimplified in conventional AHP models (Tehrany et al., 2015; Antzoulatos et al., 2022)

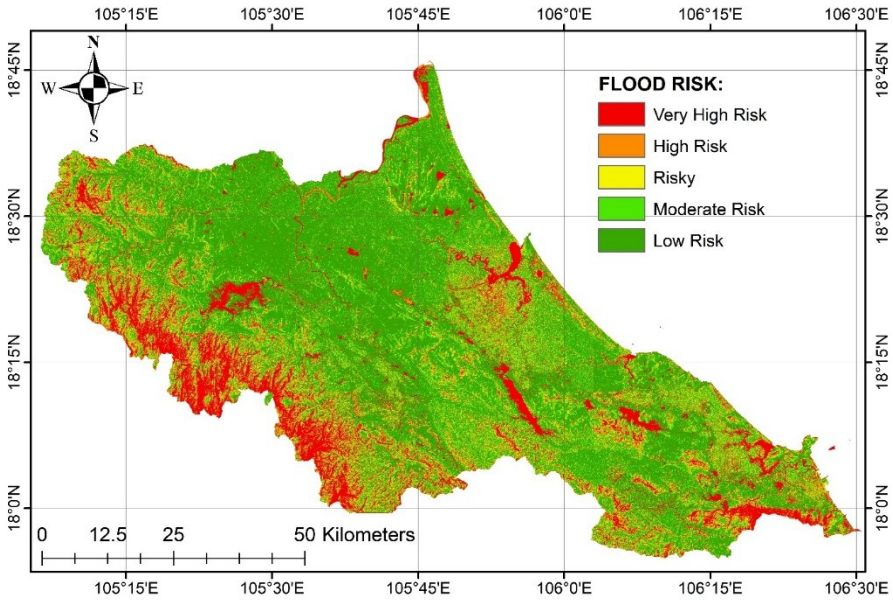

Figure 10: Flood risk map derived from AHP and AHP–SVM integration

Spatially, very high-risk areas (in red) are concentrated along major river valleys and low-lying floodplains, particularly within the La, Ngan Pho, and Ngan Sau river basins, as well as the eastern coastal corridor from Thach Ha to Ky Anh. These zones correspond to areas of high population density, agricultural concentration, and infrastructure expansion. Frequent flooding is also recorded in the western foothills of Huong Khe and Vu Quang, where steep terrain combined with localized heavy rainfall triggers flash floods and landslides.

High-risk areas (in orange) form transitional belts surrounding the very high-risk zones, primarily within the middle reaches of river systems and in peri-urban communes undergoing rapid land-use change. Moderate-risk areas (in yellow) represent mixed-use landscapes with intermediate slopes and partial vegetation cover, serving as hydrological buffers. Conversely, low and very low-risk areas (in green) dominate the elevated midland and mountainous zones, where steep slopes, high forest cover, and permeable soils enhance infiltration and reduce surface runoff.

Overall, the spatial structure of flood risk closely aligns with the province's topographic gradient and land-use dynamics. The AHP–SVM integration demonstrates high reliability for mapping complex flood patterns in mixed terrain, offering an operational tool for spatial planning and disaster risk management in central Vietnam.

3.5. Flood Risk Zonation Based on AHP–SVM Integration

The spatial distribution of flood risk across the study area demonstrates a clear west–east gradient associated with elevation, terrain morphology, and hydrological connectivity. The very high-risk zone, accounting for 3,011.27 km² (47.66%), is predominantly concentrated in low-lying coastal and deltaic communes. These areas are characterized by flat topography, low elevation, dense river–canal networks, and direct exposure to tidal influence, which collectively limit drainage efficiency and

intensify flood vulnerability. The pattern aligns with hydrological conditions and land development trends (Le et al., 2023; Nguyen et al., 2023).

Table 2. Area and percentage of flood risk levels in the study area

Level	Area (km²)	Percentage (%)
Low risk	884.14	13.99
Moderate risk	620.16	9.82
Risky	713.47	11.29
High risk	1,089.38	17.24
Very high risk	3,011.27	47.66

According to Table 2, the high-risk zone (1,089.38 km²; 17.24%) is mainly distributed across transitional mid-slope communes, where the terrain begins to rise but remains influenced by downstream flow accumulation. These areas function as receiving basins for runoff originating from upstream mountainous catchments, resulting in recurrent overbank flooding during intense rainfall. The topographic concavity and moderate slopes promote temporary water retention, explaining the spatial clustering of high-risk zones along the mid-reaches of the La, Ngan Pho, and Ngan Sau rivers.

The moderate-risk (620.16 km²; 9.82%) and risky (713.47 km²; 11.29%) zones are prevalent in intermediate elevation areas characterized by mixed land-use structures and fragmented vegetation cover. These areas partially buffer flood impacts due to infiltration capacity and vegetation interception. However, rapid urban expansion and agricultural intensification are increasing the extent of impervious surfaces, which may disrupt natural drainage networks. Without adaptive land-use control, these transitional zones are likely to experience expanding flood exposure under future rainfall extremes and sea-level rise conditions.

The low-risk zone (884.14 km²; 13.99%) is located mainly in upland communes with steeper slopes (>15°) and dense forest cover, promoting rapid surface runoff dispersion and minimizing water accumulation. Nevertheless, these regions remain vulnerable to secondary hazards such as flash floods and landslides, especially under prolonged high-intensity rainfall. The spatial gradient from low- to high-risk areas therefore reflects the combined influence of elevation, slope morphology, hydrological connectivity, and human land-use pressure within Ha Tinh’s dynamic landscape.

3.6. Model validation and performance assessment

Model validation was conducted using an independent 30% test dataset, where predicted flood risk classes from the SVM model were compared with reference samples to compute overall accuracy (OA = 0.87) and Kappa coefficient (0.81). These results confirm a high degree of reliability, indicating that the hybrid AHP–SVM

framework effectively captures nonlinear relationships among geomorphological, hydrological, and land-use factors (Congalton, 1991; Foody, 2002).

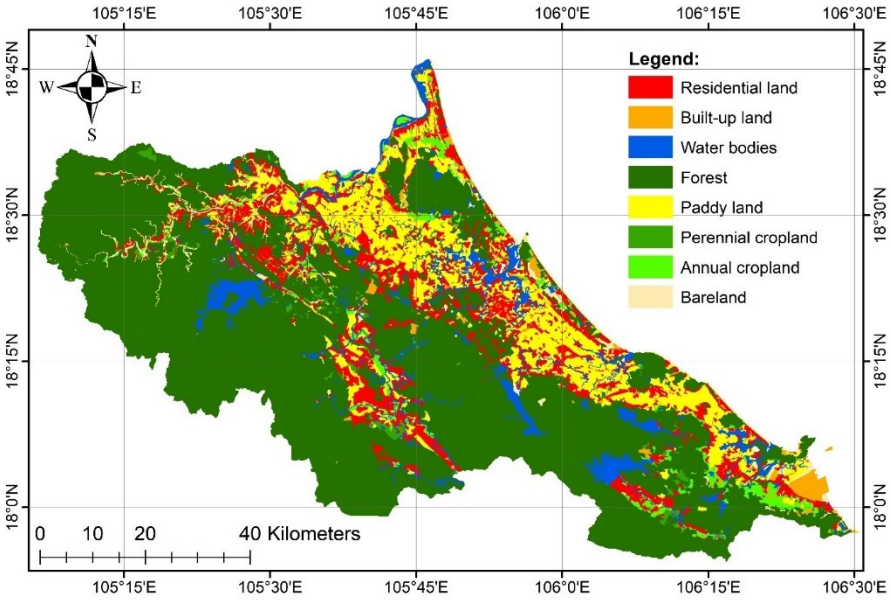

Figure 11: Land use planning map of Ha Tinh province in 2030

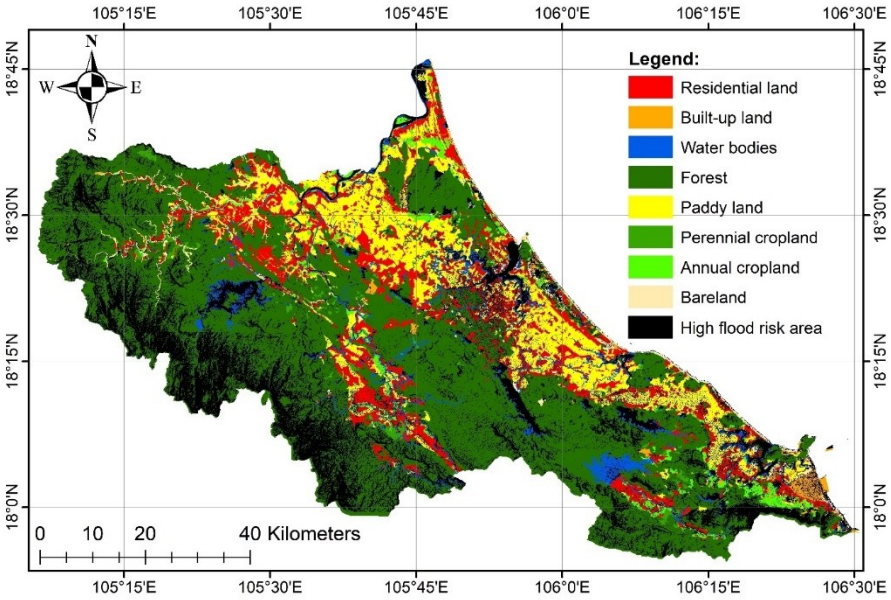

Figure 12: Spatial overlap between the 2030 land use planning and high flood risk zones in Ha Tinh province

Beyond statistical validation, spatial verification was performed by overlaying the flood risk map with the 2030 land-use planning map (Figures 11–12). The overlay analysis revealed distinct spatial conflicts between planned development zones and high flood hazard areas, particularly within the urban expansion corridor of central Ha Tinh, the coastal agricultural lowlands, and the industrial–urban coastal belt of Ky Anh. These overlapping zones represent areas of rapid land transformation where population growth, infrastructure development, and economic activities coincide with flood-prone terrain, posing significant challenges for sustainable spatial planning (Antzoulatos et al., 2022; Seydi et al., 2023; Mhangara et al., 2025; Arora et al., 2025).

Table 3. The area of land use classes according to the 2030 land use planning map of Ha Tinh province located in high flood risk zones

Class	Residential land	Built-up land	Water bodies	Forest	Paddy land	Perennial cropland	Annual cropland	Bareland
Area (km^2)	613.77	55.71	138.24	2412.12	622.83	63.87	164.03	30.08
Total	4,100.65 km^2							

According to Table 3, a total of 4,100.65 km² of planned land-use classes are located within high and very high flood-risk zones, accounting for a substantial proportion of Ha Tinh's territory. Forest land (2,412.12 km²) occupies the largest share, indicating that flood hazards extend beyond the coastal plains into mountainous and hilly catchments, where flash floods and landslides occur. Paddy land (622.83 km²) and residential land (613.77 km²) are also highly exposed, representing serious threats to food security, livelihoods, and built infrastructure if adaptive measures are not integrated into planning.

Other land-use types—annual cropland (164.03 km²), perennial cropland (63.87 km²), built-up land (55.71 km²), water bodies (138.24 km²), and bare land (30.08 km²)—occupy smaller areas but remain vulnerable due to their socio-economic importance. These findings highlight the need to embed flood risk information into land-use and regional planning frameworks, reinforcing climate-resilient zoning, adaptive infrastructure design, and ecosystem-based land management.

Overall, the integrated AHP–SVM–GIS framework not only demonstrates strong predictive performance but also provides a spatial decision-support system for reconciling development and disaster mitigation objectives. This approach offers actionable insights for local authorities to align land-use planning, climate adaptation, and disaster management strategies across Ha Tinh Province.

4. CONCLUSION

This study developed an integrated AHP–SVM–GIS framework to assess flood risk and evaluate the spatial compatibility of land-use planning in Ha Tinh Province, Vietnam. By combining expert-based weighting (AHP) and data-driven classification (SVM), the framework successfully quantified the complex interactions among topographic, hydrological, and land-use variables, providing a robust and transparent basis for flood susceptibility mapping. The results indicate that approximately 4,100.65 km² of Ha Tinh's territory falls under high or very high flood risk, with the

most affected land classes being forest land, residential areas, and paddy fields. Overlay analysis with the 2030 land-use plan revealed considerable spatial conflicts, as substantial portions of planned residential and agricultural zones coincide with flood-prone areas. These findings demonstrate that current land-use planning frameworks remain insufficiently aligned with hydro-meteorological risk realities. From a methodological perspective, the proposed AHP–SVM integration improved the accuracy, consistency, and interpretability of flood hazard mapping compared with traditional AHP-only approaches. This highlights the potential of hybrid GIS–multicriteria–machine learning models to bridge the gap between expert judgment and data analytics in spatial risk assessment. For policy and planning, the study underscores the need to embed disaster risk reduction and climate adaptation measures into land-use decision-making—through stricter control in high-risk zones, restoration of forest ecosystems, and investment in climate-resilient infrastructure. Although the current framework was applied to Ha Tinh, its methodological design is scalable and transferable to other flood-prone regions with comparable data conditions.

Future research should focus on integrating hydrodynamic simulation models, socio-economic vulnerability indicators, and climate projection scenarios, to enhance dynamic flood forecasting and adaptive spatial planning at regional scales.

REFERENCES

1. Aguarón, J., & Moreno-Jiménez, J. M. (2003). The geometric consistency index: Approximated thresholds. *European journal of operational research*, *147*(1), 137-145.
2. Al-Kindi, K. M., & Alabri, Z. (2024). Investigating the role of the key conditioning factors in flood susceptibility mapping through machine learning approaches. *Earth Systems and Environment*, *8*(1), 63-81. https://doi.org/10.1007/s41748-023-00369-7.
3. Amatebelle, C. E., Owolabi, S. T., Ogundeji, A. A., & Okolie, C. C. (2025). A systematic analysis of remote sensing and geographic information system applications for flood disaster risk management. *Journal of Spatial Science*, 1-27. https://doi.org/10.1080/14498596.2025.2476973.
4. Antzoulatos, G., Kouloglou, I.-O., Bakratsas, M., Moumtzidou, A., Gialampoukidis, I., Karakostas, A., … Kompatsiaris, I. (2022). Flood hazard and risk mapping by applying an explainable machine-learning framework using satellite imagery and GIS data. *Sustainability, 14*(6), 3251. https://doi.org/10.3390/su14063251
5. Antzoulatos, G., Kouloglou, I.-O., Bakratsas, M., Moumtzidou, A., Gialampoukidis, I., Karakostas, A., … Kompatsiaris, I. (2022). *Flood hazard and risk mapping by applying an explainable machine-learning*

framework using satellite imagery and GIS data. Sustainability, 14(6), 3251. https://doi.org/10.3390/su14063251

6. Antzoulatos, G., Kouloglou, I.-O., Bakratsas, M., Moumtzidou, A., Gialampoukidis, I., Karakostas, A., & Kompatsiaris, I. (2022). *Flood hazard and risk mapping by applying an explainable machine-learning framework using satellite imagery and GIS data.* Sustainability, 14(6), 3251.

7. Arora, A., Purna Durga, G., Pandey, M., & Arabameri, A. (2025). *Machine learning model optimization for flood susceptibility zonation over the Kosi megafan, Himalayan foreland basin, India.* Scientific Reports, 15, 32757. https://doi.org/10.1038/s41598-025-07403-w

8. Bojer, A. K., Abshare, M. W., Mesfin, F., & Al-Quraishi, A. M. F. (2025). Assessing climate and land use impacts on surface water yield using remote sensing and machine learning. *Scientific Reports*, *15*(1), 18477. https://doi.org/10.1038/s41598-025-03493-8.

9. Congalton, R. G. (1991). A review of assessing the accuracy of classifications of remotely sensed data. *Remote Sensing of Environment, 37*(1), 35–46. https://doi.org/10.1016/0034-4257(91)90048-B

10. Dang, T. T., Nguyen, H. T., & Pham, M. Q. (2022). *Rainfall variability and flood regime in north-central Vietnam under climate change scenarios.* Journal of Hydrology: Regional Studies, 43, 101147. https://doi.org/10.1016/j.ejrh.2022.101147

11. Dano Umar, L., Matori, A. N., Hashim, A. M., Chandio, I. A., Sabri, S., Balogun, A. L., & Abba, H. A. (2011). Geographic information system and remote sensing applications in flood hazards management: A review. *Research Journal of Applied Sciences, Engineering and Technology*, *3*(9), 933-947

12. Foody, G. M. (2002). Status of land-cover classification accuracy assessment. *Remote Sensing of Environment, 80*(1), 185–201. https://doi.org/10.1016/S0034-4257(01)00295-4
13. Funk, Chris, Pete Peterson, Martin Landsfeld, Diego Pedreros, James Verdin, Shraddhanand Shukla, Gregory Husak, James Rowland, Laura Harrison, Andrew Hoell & Joel Michaelsen. (2015). The climate hazards infrared precipitation with stations-a new environmental record for monitoring extremes. *Scientific Data 2,* 150066. doi:10.1038/sdata.2015.66 2015.
14. Ghosh, A., & Kar, S. K. (2018). Application of analytical hierarchy process (AHP) for flood risk assessment: a case study in Malda district of West Bengal, India. *Natural Hazards, 94*(1), 349-368. https://doi.org/10.1007/s11069-018-3392-y.
15. Glago, F. J. (2021). Flood disaster hazards; causes, impacts and management: a state-of-the-art review. *Natural hazards-impacts, adjustments and resilience*. doi: 10.5772/intechopen.95048.

16. Goodess, C. M. (2013). How is the frequency, location and severity of extreme events likely to change up to 2060?. *Environmental science & policy*, *27*, S4-S14. https://doi.org/10.1016/j.envsci.2012.04.001.
17. Goumghar, L., Fri, R., Hajaj, S., Taia, S., & El Mansouri, B. (2025). Integrating geospatial data and analytic hierarchy process for flood-prone zones mapping in the Upper Draa basin, Morocco. *Ecological Engineering & Environmental Technology (EEET)*, *26*(4). https://doi.org/10.12912/27197050/201160.
18. GSO. (2024). *Statistical Yearbook of Vietnam 2024*. General Statistics Office, Statistical Publishing House, Hanoi.
19. Gu, X., Zhang, Q., Li, J., Chen, D., Singh, V. P., Zhang, Y. & Yu, H. (2020). Impacts of anthropogenic warming and uneven regional socio-economic development on global river flood risk. *Journal of Hydrology*, *590*, 125262. https://doi.org/10.1016/j.jhydrol.2020.125262.
20. Hashim, F., Dibs, H., & Jaber, H. S. (2021, July). Applying support vector machine algorithm on multispectral remotely sensed satellite image for geospatial analysis. In *Journal of Physics: Conference Series* (Vol. 1963, No. 1, p. 012110). IOP Publishing. DOI: 10.1088/1742-6596/1963/1/012110.
21. He, F., Liu, S., Mo, X., & Wang, Z. (2025). *Interpretable flash flood susceptibility mapping in the Yarlung Tsangpo River Basin using H2O Auto-ML*. Scientific Reports, 15, 1702. https://doi.org/10.1038/s41598-024-84655-y
22. Hoang, T. V., Chou, T. Y., Nguyen, N. T., Fang, Y. M., Yeh, M. L., Nguyen, Q. H., & Nguyen, X. L. (2019). A Robust Early Warning System for Preventing Flash Floods in Mountainous Area in Vietnam. *ISPRS International Journal of Geo-Information*, *8*(5), 228. https://doi.org/10.3390/ijgi8050228.
23. Ireland, G., Volpi, M., & Petropoulos, G. P. (2015). Examining the Capability of Supervised Machine Learning Classifiers in Extracting Flooded Areas from Landsat TM Imagery: A Case Study from a Mediterranean Flood. *Remote Sensing*, *7*(3), 3372-3399. https://doi.org/10.3390/rs70303372
24. Istomina, M. N., & Dobrovoski, S. G. (2016). Floods of the world: quantitative analysis of natural characteristics and parameters of social-economic damages. *Water resources*, *43*(3), 459-471. https://doi.org/10.1134/S0097807816030076.
25. Jonkman, S. N. (2005). Global perspectives on loss of human life caused by floods. Natural hazards, 34(2), 151-175. https://doi.org/10.1007/s11069-004-8891-3.
26. Kılıç, G., & Bektaş Balçık, F. (2025). Flood-Risk Map for Büyükçekmece District Based on Socioeconomic Factors. *Environmental and Earth Sciences Proceedings*, *32*(1), 11. https://doi.org/10.3390/eesp2025032011.
27. Kiptum, A., Mwangi, E., Otieno, G., Njogu, A., Kilavi, M., Mwai, Z., & Todd, M. C. (2025). Advancing operational flood forecasting, early warning and risk management with new emerging science: Gaps, opportunities and barriers in

Kenya. *Journal of flood risk management*, *18*(1), e12884. https://doi.org/10.1111/jfr3.12884.

28. Kirshen, P., Watson, C., Douglas, E., Gontz, A., Lee, J., & Tian, Y. (2008). Coastal flooding in the Northeastern United States due to climate change. *Mitigation and Adaptation Strategies for Global Change*, *13*(5), 437-451. https://doi.org/10.1007/s11027-007-9130-5.
29. Kundzewicz, Z. W., Kanae, S., Seneviratne, S. I., Handmer, J., Nicholls, N., Peduzzi, P., Sherstyukov, B. (2013). Flood risk and climate change: global and regional perspectives. *Hydrological Sciences Journal*, *59*(1), 1-28. https://doi.org/10.1080/02626667.2013.857411.
30. Kwiesielewicz, M., & Van Uden, E. (2004). Inconsistent and contradictory judgements in pairwise comparison method in the AHP. *Computers & Operations Research*, *31*(5), 713-719. https://doi.org/10.1016/S0305-0548(03)00022-4.
31. Le, T. T. A., Lan-Anh, N. T., Daskali, V., Verbist, B., Vu, K. C., Anh, T. N., & Willems, P. (2021). Urban flood hazard analysis in present and future climate after statistical downscaling: a case study in Ha Tinh city, Vietnam. *Urban Water Journal*, *18*(4), 257-274. https://doi.org/10.1080/1573062X.2021.1877744.
32. Le, T. T. A., Willems, P., & Nguyen, L. A. (2023). Flood Hazard Analysis under Current and Future Climate Conditions for Ha Tinh Province, Vietnam. PhD Thesis.
33. Loi, D. T., Huong, L. V., Tuan, P. A., Hong Nhung, N. T., Quynh Huong, T. T., & Hoa Man, B. T. (2022). An Assessment of Agricultural Vulnerability in the Context of Global Climate Change: A Case Study in Ha Tinh Province, Vietnam. *Sustainability*, *14*(3), 1282. https://doi.org/10.3390/su14031282.
34. Mazziotta, M., & Pareto, A. (2022). Normalization methods for spatio-temporal analysis of environmental performance: Revisiting the Min–Max method. *Environmetrics*, *33*(5), e2730. https://doi.org/10.1002/env.2730.
35. Mhangara, P., Gidey, E., & Mbazo, M. (2025). Flood hazard monitoring and modeling systems for improving climate risk management using machine learning and geospatial models in the Hennops River catchment, Centurion, South Africa. *Discover Sustainability, 6*, 2. https://doi.org/10.1007/s43621-024-00735-z
36. MONRE. (2024). *National Land Resource and Land Use Report 2024: Provincial land structure of Vietnam*. Ministry of Natural Resources and Environment, Hanoi
37. Munier, N., & Hontoria, E. (2021). *Uses and Limitations of the AHP Method*.
38. Nguyen, D. L., Chou, T. Y., Hoang, T. V., & Chen, M. H. (2023). Flood susceptibility mapping using machine learning algorithms: a case study in Huong Khe District, Ha Tinh Province, Vietnam. *International Journal of Geoinformatics*, *19*(7), 1-15.
39. Nguyen, D. L., Tran, M. H., & Le, V. T. (2024). *Flood susceptibility mapping using machine learning algorithms: Comparative analysis of SVM, RF, and ANN models.* International Journal of Geo-Information, 13(4), 2739.

https://ijg.journals.publicknowledgeproject.org/index.php/journal/article/download/2739/1523

40. Nguyen, H. D. (2023). Spatial modeling of flood hazard using machine learning and GIS in Ha Tinh province, Vietnam. *Journal of Water and Climate Change, 14*(1), 200-222. doi: 10.2166/wcc.2022.257.
41. Nguyen, L. D., Nguyen, H. T., Dang, P. D., Duong, T. Q., & Nguyen, L. K. (2021). Design of an automatic hydro-meteorological observation network for a real-time flood warning system: a case study of Vu Gia-Thu Bon river basin, Vietnam. *Journal of Hydroinformatics*, *23*(2), 324-339. https://doi.org/10.2166/hydro.2021.124.
42. Nguyen, T. H., & Pham, H. V. (2022). *Forest ecosystem services for watershed protection in the upper catchments of Ha Tinh Province.* Vietnam Journal of Forestry Science, 9(2), 45–58.
43. Ortiz-Vargas, A.; Sebesvari, Z. (2021). Technical Report: Floods in Central Viet Nam. In *Interconnected Disaster Risks 2020/2021*; United Nations University-Institute for Environment and Human Security (UNU-EHS): Bonn, Germany.
44. Perera, D., Agnihotri, J., Seidou, O., & Djalante, R. (2020). Identifying societal challenges in flood early warning systems. *International Journal of Disaster Risk Reduction*, *51*, 101794. https://doi.org/10.1016/j.ijdrr.2020.101794.
45. Pham, B. T., Phong, T. V., Nguyen, H. D., Qi, C., Al-Ansari, N., Amini, A., Ho, L. S., Tuyen, T. T., Yen, H. P. H., Ly, H.-B., Prakash, I., & Tien Bui, D. (2020). A Comparative Study of Kernel Logistic Regression, Radial Basis Function Classifier, Multinomial Naïve Bayes, and Logistic Model Tree for Flash Flood Susceptibility Mapping. *Water*, *12*(1), 239. https://doi.org/10.3390/w12010239.
46. Pham, N. T. T., Nguyen, Q. H., Ngo, A. D., Le, H. T. T., & Nguyen, C. T. (2018). Investigating the impacts of typhoon-induced floods on the agriculture in the central region of Vietnam by using hydrological models and satellite data. *Natural Hazards*, *92*(1), 189-204. https://doi.org/10.1007/s11069-018-3202-6.
47. Pham, T. H., Tran, P. T., & Le, D. N. (2023). *Application of AHP–GIS for flood susceptibility mapping in Quang Binh Province, Vietnam.* Environmental Challenges, 10, 100752. https://doi.org/10.1016/j.envc.2023.100752
48. Rajkhowa, S., & Sarma, J. (2021). Climate change and flood risk, global climate change. In *Global climate change* (pp. 321-339). Elsevier. https://doi.org/10.1016/B978-0-12-822928-6.00012-5.
49. Ringo, J., Sabai, S., & Mahenge, A. (2025). Contribution of flood early warning response measures in reducing flood effects in Kilosa District, Tanzania. *Climate Services*, *37*, 100534.
50. Sabzi, H. Z., & King, J. P. (2015). Numerical comparison of multi-criteria decision-Making techniques: A simulation of flood management multi-criteria systems. In *World Environmental and Water Resources Congress 2015* (pp. 359-373).
51. Sato, Y., & Tan, C. W. (2023). *Assessing consistency in multi-criteria decision-making: Improved evaluation of the AHP method.* Environmental Modelling & Software, 163, 105645. https://doi.org/10.1016/j.envsoft.2023.105645

52. Seydi, S. T., Kanani-Sadat, Y., Hasanlou, M., Sahraei, R., Chanussot, J., & Amani, M. (2023). Comparison of machine learning algorithms for flood susceptibility mapping. *Remote Sensing*, *15*(1), 192. https://doi.org/10.3390/rs15010192
53. Singh, D., & Singh, B. (2022). Feature wise normalization: An effective way of normalizing data. *Pattern Recognition*, *122*, 108307. https://doi.org/10.1016/j.patcog.2021.108307.
54. Singha, C., Chakraborty, N., Sahoo, S., Pham, Q. B., & Xuan, Y. (2025). A novel framework for flood susceptibility assessment using hybrid analytic hierarchy process-based machine learning methods. *Natural Hazards*, 1-46. https://doi.org/10.1007/s11069-025-07335-8.
55. Svetlana, D., Radovan, D., & Ján, D. (2015). The economic impact of floods and their importance in different regions of the world with emphasis on Europe. *Procedia Economics and Finance*, *34*, 649-655. https://doi.org/10.1016/S2212-5671(15)01681-0.
56. Tehrany, M. S., Pradhan, B., Mansor, S., & Ahmad, N. (2015). Flood susceptibility assessment using GIS-based support vector machine model with different kernel types. *Catena*, *125*, 91-101. https://doi.org/10.1016/j.catena.2014.10.017.
57. Thammaboribal, P., Triapthti, N. K., & Lipiloet, S. (2025). Using of Analytical Hierarchy Process (AHP) in Disaster Management: A Review of Flooding and Landslide Susceptibility Mapping. *International Journal of Geoinformatics*, *21*(4), 177-196. https://doi.org/10.52939/ijg.v21i4.4091.
58. Tran, M. V., Nguyen, T. T., & Le, V. H. (2021). *Topographic characteristics and river networks of Ha Tinh Province for disaster zoning.* Vietnam Journal of Meteorology and Hydrology, 727, 43–52.
59. Ullah, M., Murtaza, G., & Ashraf, M. (2025). Socio-Economic and Environmental Impacts of Flood 2010 in Lower Dir District and Mitigation Measures. *Journal of Management & Social Science*, *2*(2), 556-573.
60. Vo, N. T., Le, V. T., & Nguyen, D. T. (2022). *Impacts of land use conversion on floodplain dynamics in Ha Tinh Province, Vietnam.* Hydrological Processes, 36(9), e14620. https://doi.org/10.1002/hyp.14620
61. Wang, X., & Xie, H. (2018). A Review on Applications of Remote Sensing and Geographic Information Systems (GIS) in Water Resources and Flood Risk Management. *Water*, *10*(5), 608. https://doi.org/10.3390/w10050608.
62. Wang, Y., Zhang, P., Xie, Y., Chen, L., & Li, Y. (2025). Toward explainable flood risk prediction: Integrating a novel hybrid machine learning model. *Sustainable Cities and Society*, *120*, 106140. https://doi.org/10.1016/j.scs.2025.106140.
63. Xu, C., Rahman, M., Haase, D., Wu, Y., Su, M., & Pauleit, S. (2020). Surface runoff in urban areas: The role of residential cover and urban growth form. *Journal of Cleaner Production*, *262*, 121421. https://doi.org/10.1016/j.jclepro.2020.121421.

64. Yin, Z., Hu, Y., Jenkins, K., He, Y., Forstenhäusler, N., Warren, R. & Guan, D. (2021). Assessing the economic impacts of future fluvial flooding in six countries under climate change and socio-economic development. *Climatic Change*, *166*(3), 38. https://doi.org/10.1007/s10584-021-03059-3.
65. Zha, D., Bhat, Z. P., Lai, K. H., Yang, F., Jiang, Z., Zhong, S., & Hu, X. (2025). Data-centric artificial intelligence: A survey. *ACM Computing Surveys*, *57*(5), 1-42. https://doi.org/10.1145/3711118.
66. Zhou, Q., Teng, S., Situ, Z., Liao, X., Feng, J., Chen, G. & Lu, Z. (2023). A deep-learning-technique-based data-driven model for accurate and rapid flood predictions in temporal and spatial dimensions. *Hydrology and Earth System* Sciences, 27(9), 1791-1808. https://doi.org/10.5194/hess-27-1791-2023, 2023.
67. Forman, E. H., & Gass, S. I. (2001). The Analytic Hierarchy Process—An exposition. Operations Research, 49(4), 469–486.
68. Luu, T. T., Nguyen, T. H., & Dang, H. T. (2020). Integration of GIS and AHP for flood hazard mapping: A case study in Central Vietnam. Natural Hazards, 104(2), 1867–1888.
69. Rahmati, O., Zeinivand, H., & Bui, D. T. (2021). A comparison of different machine learning models for flood susceptibility mapping: A case study of the Haraz watershed, Iran. Science of the Total Environment, 788, 147659.
70. Saaty, T. L. (2008). Decision making with the Analytic Hierarchy Process. International Journal of Services Sciences, 1(1), 83–98.
71. Vargas, L. G. (2010). Models, methods, concepts & applications of the Analytic Hierarchy Process (2nd ed.). Springer